Report on HQ02 Cross Section Analysis

Andrea Carbonara and Trey Holik

I. Abstract

The US LHC Accelerator Research Program (LARP) quadrupole HQ02 was designed and fully tested as part of the low-beta quad development for Hi-Lumi LHC. HQ02's design is well documented with full fabrication accounting along with full field analysis at low and high current. With this history, HQ02 is an excellent test bed for developing a methodology for measuring turn locations from magnet cross sections and comparing with CAD models and measured field. All 4 coils of HQ02 were cut in identical locations along the magnetic length corresponding to magnetic field measurement and coil metrology. A real-time camera and coordinate measuring equipment was used to plot turn corners. Measurements include systematic and random displacements from nominal and waviness of winding blocks and individual turns along the magnetic length. The level of conductor displacement and waviness when compared to the measured RMS harmonics are in agreement, although correlating turn locations and measured harmonics in each cross sections is challenging.

II. Introduction

Hi-Lumi LHC requires ultra-high performance Nb_3Sn quadrupoles for squeezing the beam at collision points. The integrated luminosity of the LHC is slated to increase by a factor of 10 by 2025 [1]. LARP has been gradually developing quadrupoles for Hi-Lumi LHC since 2004 [2]. HQ02 was an intermediate generation magnet with 120-mm aperture to test several aspects of superconducting quadrupole construction and operation [3 - 5].

The magnetic field harmonics of HQ02 were measured along the length of the magnet after magnet assembly and at full field [6, 7]. Afterwards, all 4 coils of the magnet were cut at specific locations along the length coinciding with magnetic field measurements. The goal of this work was twofold: to collect data about coil cross section in order to quantify turn locations and displacements longitudinally, and to use these data to assess the role of conductor location and displacement on field quality. Ultimately the measured field quality during magnet testing will be compared to the calculated field quality from magnet cross sections.

This report intends to explain the methods used to collect and process data and to present and discuss the results. For further clarification and corrections, please refer to the authors at andrea.carbonara@mail.polimi.it and eholik@fnal.gov.

III. Coil CMM

All HQ02 coils were analyzed with a Coordinate Measurement Machine or CMM before magnet assembly at LBNL and before cutting at BNL. The coils were universally oversize by an average of 40 µm and were accommodated by removing radial shim.

The CMM data from BNL revealed that the coils slightly shrank during cold testing so that each coil was undersize by an average of 55 µm along the straight section of each coil. On average the left (transition side) midplane was smaller than the right by 24 µm. The standard deviation on coil size was 60 µm and the standard deviation on midplane asymmetry was 51 µm.

IV. Data Collection – Single Coil

Here we describe the steps for measuring turn location for a single coil. The instrument used was an Optical Comparator (Optical Gauging Products), which can measure and store the 2D position of points on a plane with a systematic error less than three µm. The random error computed as a 1-sigma distance from average from repeated measurements of the same coil cross section is 12 µm.

A. Reference Frame Identification

The first step after positioning the coil segment on the instrument is to collect data about the outer diameter (from now on, OD) and the keyway sides by an automatic edge detection feature built in the instrument. It collected data on the edges with a spacing of 250 µm. Points on the OD were used to define the center of the reference frame, by fitting the points to a circle of imposed radius R = 91.472 mm, the nominal HQ coil OD. The center of the circle is found by minimizing

$$\min_{x_0,y_0} \sum_i (x_i - x_0)^2 + (y_i - y_0)^2 - R^2 \quad (1)$$

where x_0 and y_0 are the two variables minimized representing the center of the circle. The sides of the keyway where used to define a 45° line in the first quadrant of the reference frame. The line was defined by two points: the center of the reference frame (defined by the OD points) and the center of the keyway, defined as the midpoint between the barycenters of the two sides of the keyway. The barycenter of each side is computed as the average of the coordinates of the point of the side itself. Each point subsequently collected is in this coil OD and Keyway best fit coordinate system. See Fig. 1 below.

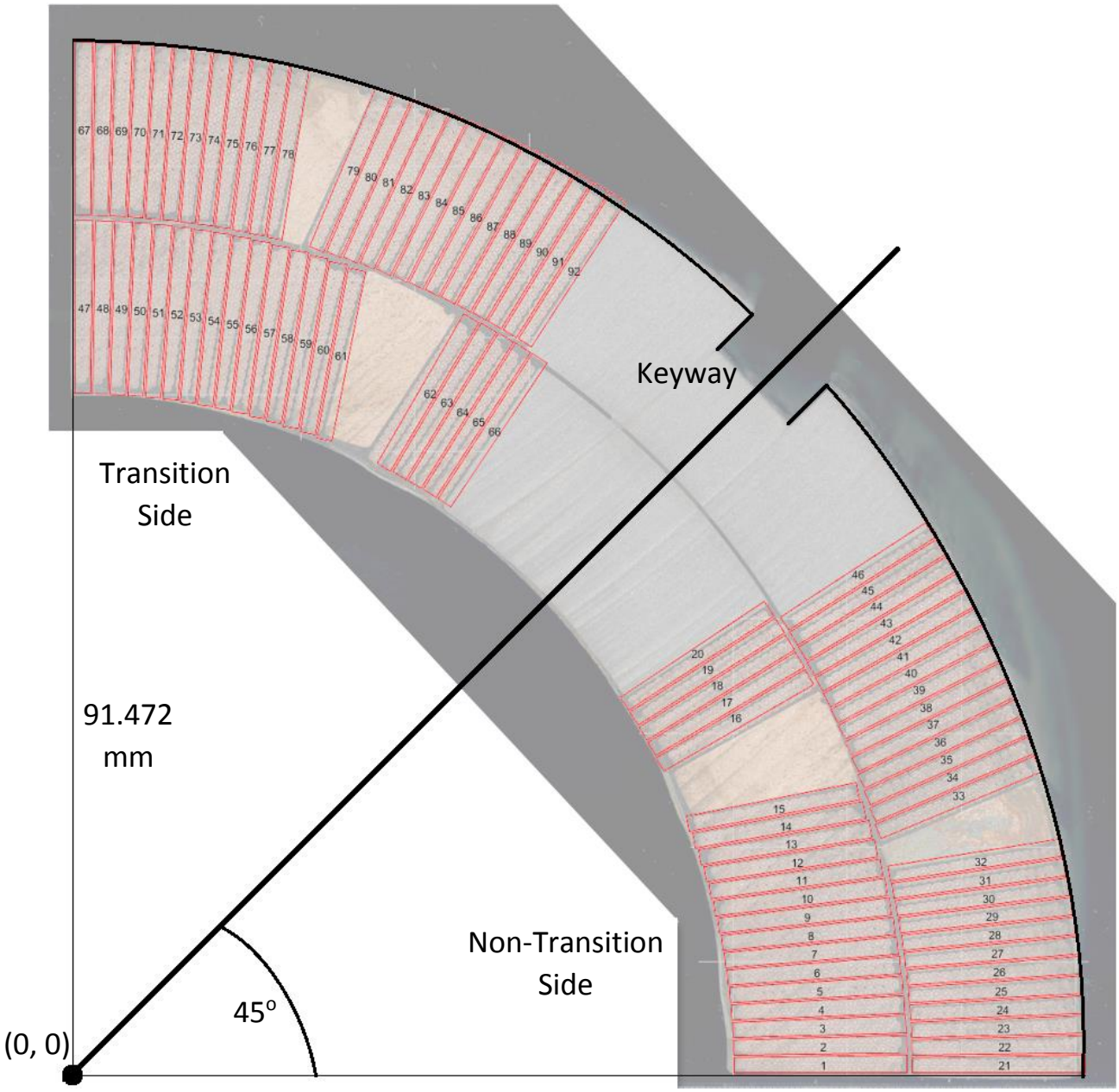

Fig. 1. Numbering scheme for the each turn of each coil and the defined coordinate system.

B. Turn Location Measurement

The four corners of each turn were collected as points. A protractor with perpendicular lines was used to identify each corner in the following way: first, pushing one line to be tangent to the longer edge of the cable and then without rotation, the protractor was shifted until the second line was tangent to one strand of the shorter edge. In this process, some issues were encountered due to: not perfect alignment of strands, not perfectly sharp edge of strands, increased cable thickness from the second/third strand due to insulation layer between the strands (core), and varying strand triplets at some turn edges. The same cross section was measured multiple times with an Root-Mean-Square distance between each measurement of 12 µm. An example of defining a cable edge is seen in Fig. 2.

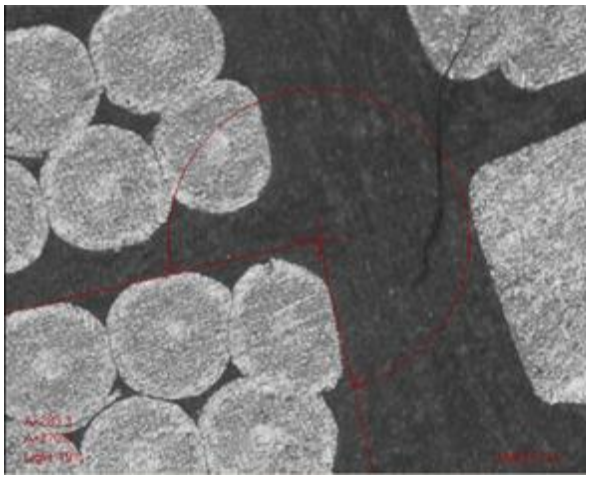

Fig. 2. Demonstration of defining the corner of one cable.

C. Numbering Scheme and Nomenclature

Turns are distributed over two layers. The internal, inner layer is defined as L1 and the external, outer layer as L2. On one side of each coil during winding, one turn transitions from L1 to L2. This determines the orientation of each coil and is referred to the transition (T) side of each cross section as indicated. Turns for the non-transition (NT) side are numbered from 1 to 46, starting from L1 turns from midplane to pole, then L2 turns from midplane to pole. Turns for T side are numbered from 47 to 92, starting from L1 midplane to pole and then L2 midplane to pole. Each of the four sectors are divided in two groups by the wedge. The four corners are ordered as in Figs. 3 and 4 below.

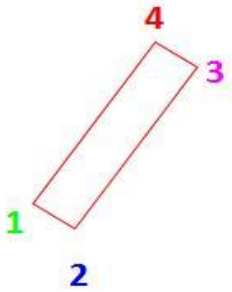

Fig. 3. Numbering scheme for the Non-Transition side.

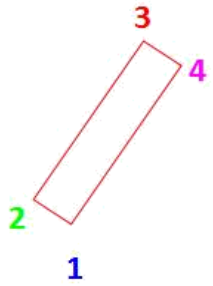

Fig. 4. Numbering scheme for the Transition side

D. Fitting points to the nominal cross section

When comparing two sides of a single cut, the turns did not overlay but rather had a systematic average shift of 150 µm. This shift suggests that the process of setting the reference frame according to the coil OD and keyway was not repeatable for different cross sections.

The process of fitting points to a nominal cross section turned to provide better results when comparing the two sides of a single cut. The nominal cross section for HQ02 coils was defined in ROXIE with the parameters given in Fig. 5.

No	Type	NCab	X	Y	α	Current	Cable name	N1	N2
1	Cos	12	75.986	0.1061	0	14000	HQ_KC4_45	2	17
2	Cos	14	75.986	15.7867	22.5778	14000	HQ_KC4_45	2	17
3	Cos	15	60.128	0.13369	0	14000	HQ_KC4_45	2	17
4	Cos	5	60.128	26.2084	30.009	14000	HQ_KC4_45	2	17

Fig. 5. ROXIE parameters for HQ02 coil cross sections and determining the nominal turn positions.

In order to modify points to the nominal cross section a rigid roto-translation was applied to points and a residual was minimized with respect to a rigid translation of (x_0, y_0) and a rotation of θ. The residual minimized is:

$$\min_{x_0,y_0,\theta} \sum_i \left(x_{2,i} - x_{i,nom}\right)^2 + \left(y_{2,i} - y_{i,nom}\right)^2 \tag{2}$$

$$x_{2,i} = x_{1,i}\cos(\theta) + y_{1,i}\sin(\theta) \tag{3}$$

$$y_{2,i} = -x_{1,i} sin\cos(\theta) + y_{1,i}\sin(\theta) \tag{4}$$

$$x_{1,i} = x_i + x_0 \tag{5}$$

$$y_{1,i} = y_i + y_0 \tag{6}$$

where x_i and y_i are the collected point coordinates and $x_{i,nom}$ and $y_{i,nom}$ are the nominal coil coordinates. It should be emphasized here that the points are not scaled. This method is sufficiently repeatable when applied to the same coil cross section surface, giving center points with a standard deviation of 10 µm.

E. Coils Analyzed

Data for single coils was collected for coils HQ17 and HQ20 @ z = -5, -105, -205 mm where z is the axis of the bore. The axial origin at z = 0 is located at the magnetic center of the assembly and +z points towards the lead end. The section labeling scheme is indicated in Fig. 6.

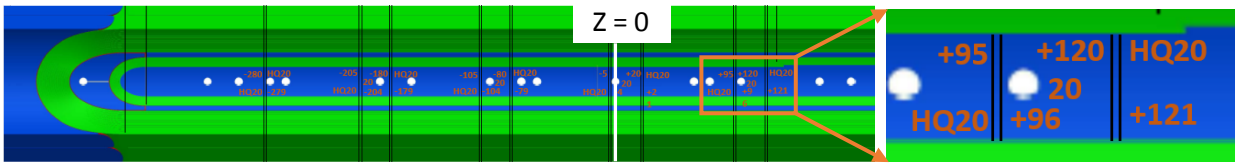

Fig. 6. HQ02 Cross Section Cuts. Field measurements correspond to z = -205, -105, -5, and +95 mm. Smaller sections were cut for automated polishing and subsequent analysis at the conductor level. All segments were water jet cut at BNL. Segments from z = -279 to -5 mm were shipped to FNAL, segments from z = -5 to +120 mm were shipped to LBNL, and the ends remain at BNL.

V. Data Collection – Collared Cross Sections

Three full cross section have been assembled using coils HQ17, HQ16, HQ15, HQ20 from the first quadrant counterclockwise. The four coils were assembled with four collars using the same parameters as during the actual HQ02b coil pack assembly. The four collars are fastened together with ¼-20 bolts and tightened to 100 in-lbs of torque, the same value as coil pack assembly. The cross sections analyzed were at z = -5, -79, -105 mm. For z -79 mm, the cross section was analyzed from the return end of the magnet, so points were inverted to have the correct 'from the lead end' orientation.

The rationale for collecting data from a full collared cross section is four fold:

1. After being water jet cut, the coils tend to flair outward increasing the effective outer radius. The collars place the coils back into the original shape and outer radius.
2. The relative position of each coil is captured when fully assembled.
3. When using the collars, determining a coordinate system is independent of coil deformation and can be based on collar position rather than OD and keyway.
4. Furthermore, rigid motion of all 4 coils have minimal effect on the calculated harmonics. For example, a full 1 mm translation only contributes at most half a unit of any harmonic.

A. Reference Frame Identification

The process for collecting data on four collared coils is very much the same as collecting data from a single coil. Here we only highlight the differences.

All previous considerations apply to the process of collecting data points, except for reference frame setting. For single coils the outer diameter and the keyway determined the reference frame for collecting data. For collared coils the four keyways alone were used for determining the reference frame without analyzing the OD. First the center of each keyway for each coil was computed as for single coils. Then two lines were created by connecting opposite keyway centers. The intersection of these two lines determines the origin. The keyway in quadrant one determines the 45° line for the full coordinate system. The orientation of all coils are shown in Fig. 7.

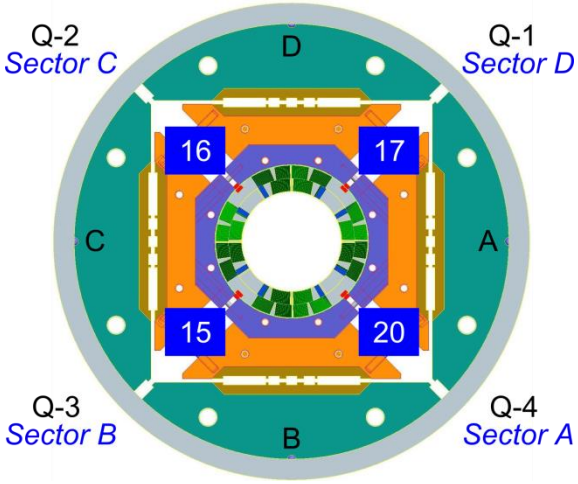

Fig. 7. HQ02 coils in the proper orientation as viewed from the lead end. A, B, C, D are marked on the magnet yoke.

B. Effect on Coil Shape from Collaring

Four coil sections (HQ17, HQ20 at Z = -5, -105) were measured with and without collaring to determine the deformation that occurs. Each cross section was best fit with the nominal cross section. The plots below represent the average shift of each turn from the collaring process.

The turns near the pole were largely unaffected as can be seen that the shift of turn 20 for Layer 1 and 26 for Layer 2 are close to zero for both the radial and azimuthal shifts. The midplane turns shift radially inward as the coils conformed to the collar ID. Additionally the collars apply a slight azimuthal pressure on each coil cross section from the collar fasteners. The ¼”-20 collar fasteners were tightened to 100 inch lbs. of torque producing approximately 2000 lbs (9000 N) azimuthal force on the coils. This equates to roughly 4 MPa of azimuthal pressure on the coils. Assuming the coil modulus is 20 GPa this would produce

30 µm of azimuthal compression for each coil. The plot indicates that each coil is actually compressing by 40 µm total or between 20 µm and 30 µm for each side.

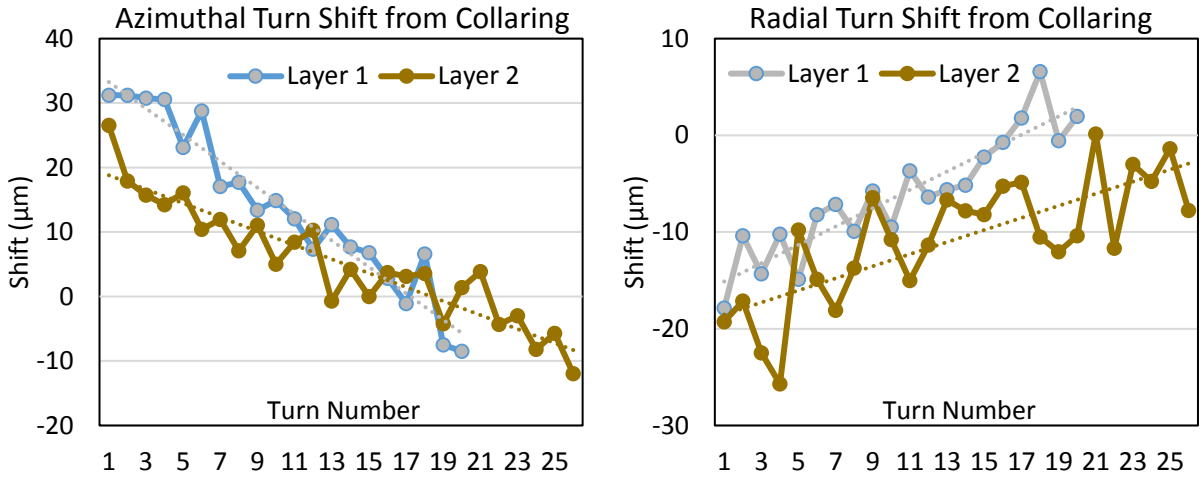

Fig. 8. Average azimuthal and radial turn shift from the collaring process

VI. Turn Location Analysis

A. Data Processing

For each coil cross section, several data has been calculated: cable radial and azimuthal displacement wrt the nominal cross section, cable width and expansion during heat treatment, and cable thickness. Each calculation is performed also on the nominal HQ02 cross section, to allow for calculating differences between measured coils and the nominal one.

Minor and major edge midpoint For each turn, the midpoint of the minor edge (the internal one) and the major edge (the external one) was calculated. In the formulas, corners numbers follow the scheme reported in Fig. 3 and 4.

$$x_{MinEdge;Mdp} = \frac{x_1+x_2}{2} \tag{7}$$

$$y_{MinEdge;Mdp} = \frac{y_1+y_2}{2} \tag{8}$$

$$x_{MajEdge;Mdp} = \frac{x_3+x_4}{2} \tag{9}$$

$$y_{MajEdge;Mdp} = \frac{y_3+y_4}{2} \tag{10}$$

Defining the cable dimension and location in this way reduces the dependence on how each cable edge was measured or plotted. As long as each cable edge was measured in repeatable manner, this averaging will accurately determine the minor and major cable edge.

Midpoint displacements For each midpoint, the displacement with respect to the nominal cross section is computed. The displacement is computed in the radial and azimuthal direction, instead of x and y direction. To do that, the position of each midpoint is transformed in polar coordinates according to: $R^2 = x^2 + y^2$ and $\theta = atan2(y, x)$. Then the displacement with respect to nominal is calculated between the polar coordinates.

$$\Delta R = R_i - R_{i,nom} \tag{11}$$

$$\Delta\theta = \theta_i - \theta_{i,nom} \tag{12}$$

$$\Delta\theta_{dist} = \Delta\theta R_{i,nom} \tag{13}$$

Finally, for each midpoint the azimuthal displacement is multiplied by the radial position of the corresponding midpoint in the nominal cross section, in order to have a distance unit for the displacement. The nominal radius was chosen for determining the change in azimuthal distance so the radial and azimuthal component are truly decoupled for calculation. So the azimuthal displacement is not a difference of angular position of the two points but is an actual displacement in the normal direction. The displacement is defined as positive from midplane to pole, so its positive direction is different according to the turn being on the T or NT side. This makes systematic displacements much easier to analyze. Cable width expansion is computed from the distance between the two midpoints. Cable expansion is computed as follows:

$$\%\, Expansion = \frac{w - w_{ref}}{w_{ref}} * 100\% \tag{14}$$

The reference width is the pre-heat treatment width for each turn and coil. Cable for HQ17 was measured at 14.760 mm and cable for all other coils was measured at 14.763 mm before coil fabrication. Determining cable thickness deviation is not statistically relevant due to the uncertainty of individual measurements.

B. Cable Width

The turns are divided into four blocks: the Transition/Non-Transition side and Layer 1/Layer 2. The different colors represent a different coil cross section, according to the legend. The plots clearly show the different level of expansion between coil HQ17 and the other coils. Coil HQ17 used cable with braided on insulation while the other coils used cable with sock type insulation. The braided on insulation constricts the cable and reduces the expansion during heat treatment.

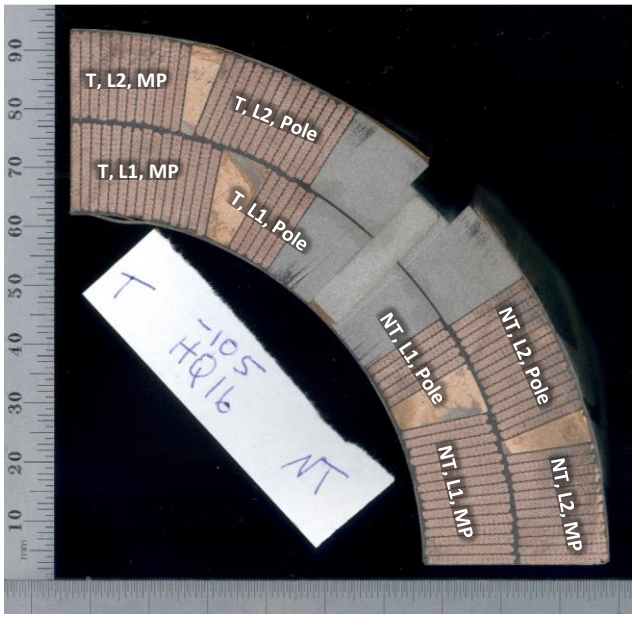

Fig. 9. Labeling scheme of each coil block for HQ02 coils.

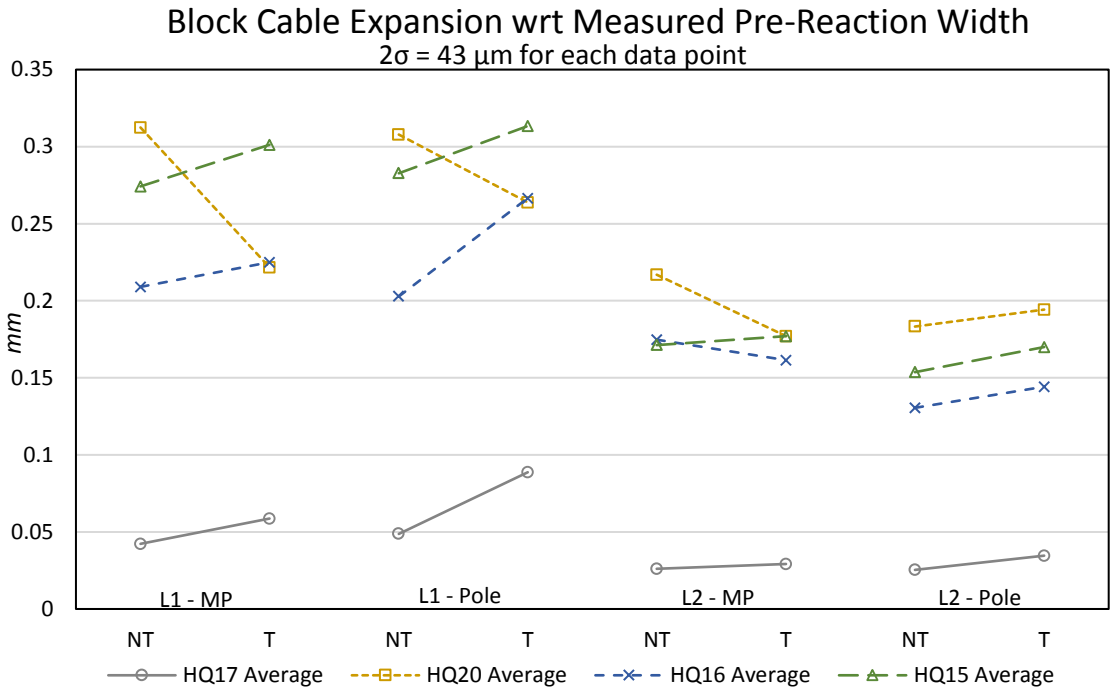

Fig. 10. Cable width expansion during heat treatment relative to the measured manufactured cable width. HQ17 was reacted with braided on insulation while all other coils were reacted with sock type insulation.

Statistical significance of the difference between coils in Fig. 10 is evaluated. The average expansion and the standard deviation is computed for each type of coil. HQ Coil 17 with braided on insulation expanded 0.27% with a standard deviation of 0.19%. HQ coil 20 with sock type insulation expanded 1.54% with a standard deviation of 0.37%. Moreover, variance of expansion between each turn is much less for HQ17. Implying that the braided on insulation might enable a more reliable dimension to use for design.

The reduced expansion in L2 for sock type coils is consistent with the hypothesis that the turns tend to press into and align along the OD. The L1 turns press into the L2 turns and reduce the measured expansion.

C. Radial, Azimuthal, and Rotational Block and Turn Displacements

The section presents measured displacements with respect to the nominal position for each turn and each block. Three distinct types of displacement are predominant in shell type windings: radial (ΔR), Azimuthal (Δθ), and rotational (ΔRot). Demonstrations of these types of displacements are shown in Fig. 11.

All displacements tend to be minimal near the midplane and near the pole indicating that the tooling and pole parts are correctly locating neighboring turns. The displacements shown in Fig. 11 as well as the displacements given in TABLE I are all based on averages of whole blocks and individual turns. The peak azimuthal and rotational displacement in the center turns is therefore typically 1.5 times larger than the average.

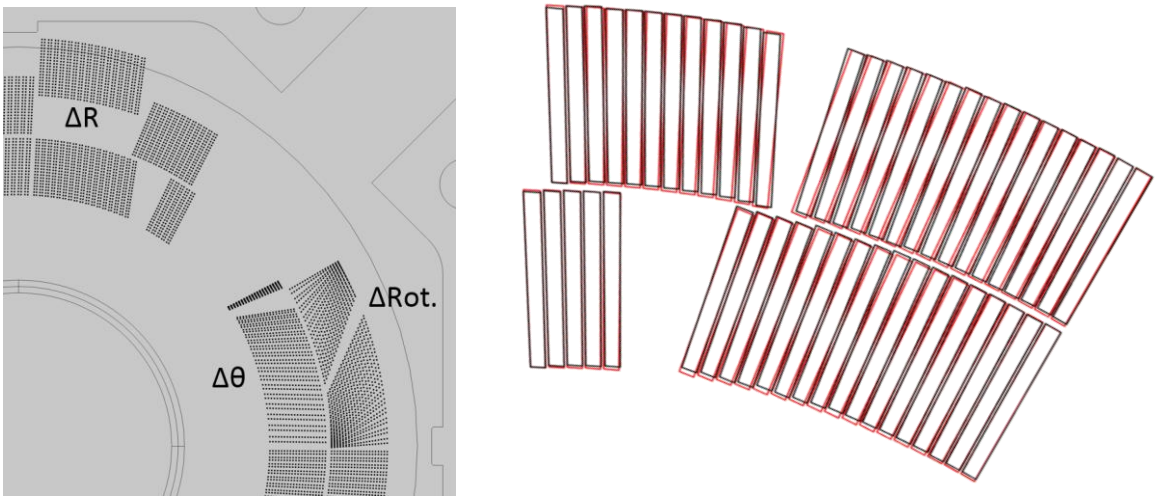

Fig. 11. Demonstration of typical displacements measured in shell type coils. The red rectangles represent the designed nominal location of each turn. The black boxes represent the measured location of each turn after a best fit with nominal.

TABLE I: Displacements of Each Block and Turn

		Braid (Coil 17)			Sock (Coils 15, 16, & 20)		
		Radial (μm)	Azimuthal (μm)	Rotation (μm)	Radial (μm)	Azimuthal (μm)	Rotation(μm)
Block	Displacement from Nominal	59	125	118	67	111	67
RMS	Displacement from Average	46	36	84	52	48	34
Turn	Displacement from Nominal	156	138	131	127	114	80
RMS	Displacement from Average	116	46	96	107	49	42

The RMS displacement from nominal is with respect to the ROXIE model. The RMS displacement from average is with respect to the average position of all coils. Rotation is the average distance that each edge of the cable is shifted in opposite directions as indicated in Fig. 11.

The average block displacements are presented in Fig. 12. All block displacement for each coil is less than 250 μm. The largest displacement is the azimuthal shift of the L2 pole block at an average of 183 μm and a peak of 240 μm for the T side of the L2 pole block of HQ17. The average shift in all plots is zero due to the 'best fit' coordinate system procedure.

Differences in displacement between the T and NT side blocks give good indication for the coil asymmetry. The peak difference between the T an NT side is in the radial direction for the L1 pole block of HQ16 at a magnitude of 134 μm. The Root-Mean-Square (RMS) difference between the NT and T sides is 42 μm, 27 μm, and 35 μm for the radial, azimuthal, and rotational displacements.

The average turn displacements for each coil are presented in Fig. 13. Radial displacement has a large standard deviation when compared to the azimuthal displacement because each turn is radially independent. The L2 radial position variation is less than L1 since the outer turns tend to press outward against the precision OD tooling while the inner turns press against the varying outer turns. The L1 and L2 radial standard deviation is 79 and 144 μm respectively.

Azimuthal displacement is quite continuous with jumps occurring at wedges. The average azimuthal L1 wedge jump is 113 μm and the average L2 wedge jump is 228 μm. The peak jump occurs in HQ17 where the L2 wedge jump is 293 μm. The cause of this large wedge jump is likely 2-fold: additional insulation on each wedge on the order of 100 μm (125 μm nominal, 175 μm measured) and the reduced cable width expansion of HQ17 allowing cable to reside on the thicker outer part of the wedge.

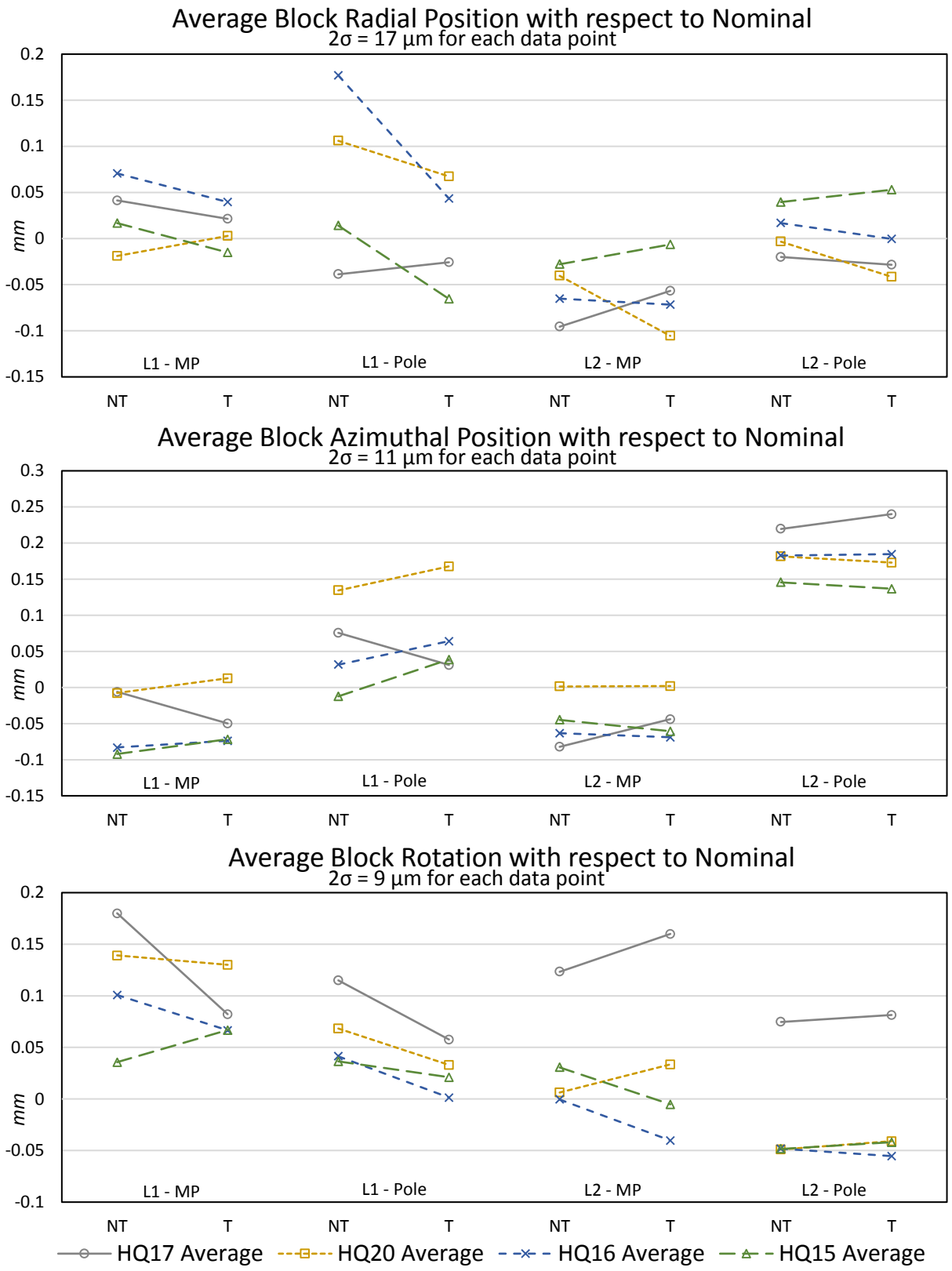

Fig. 12. Average radial, azimuthal, and rotational block displacements with respect to the nominal position. The 95% confidence level for each measurement is indicated.

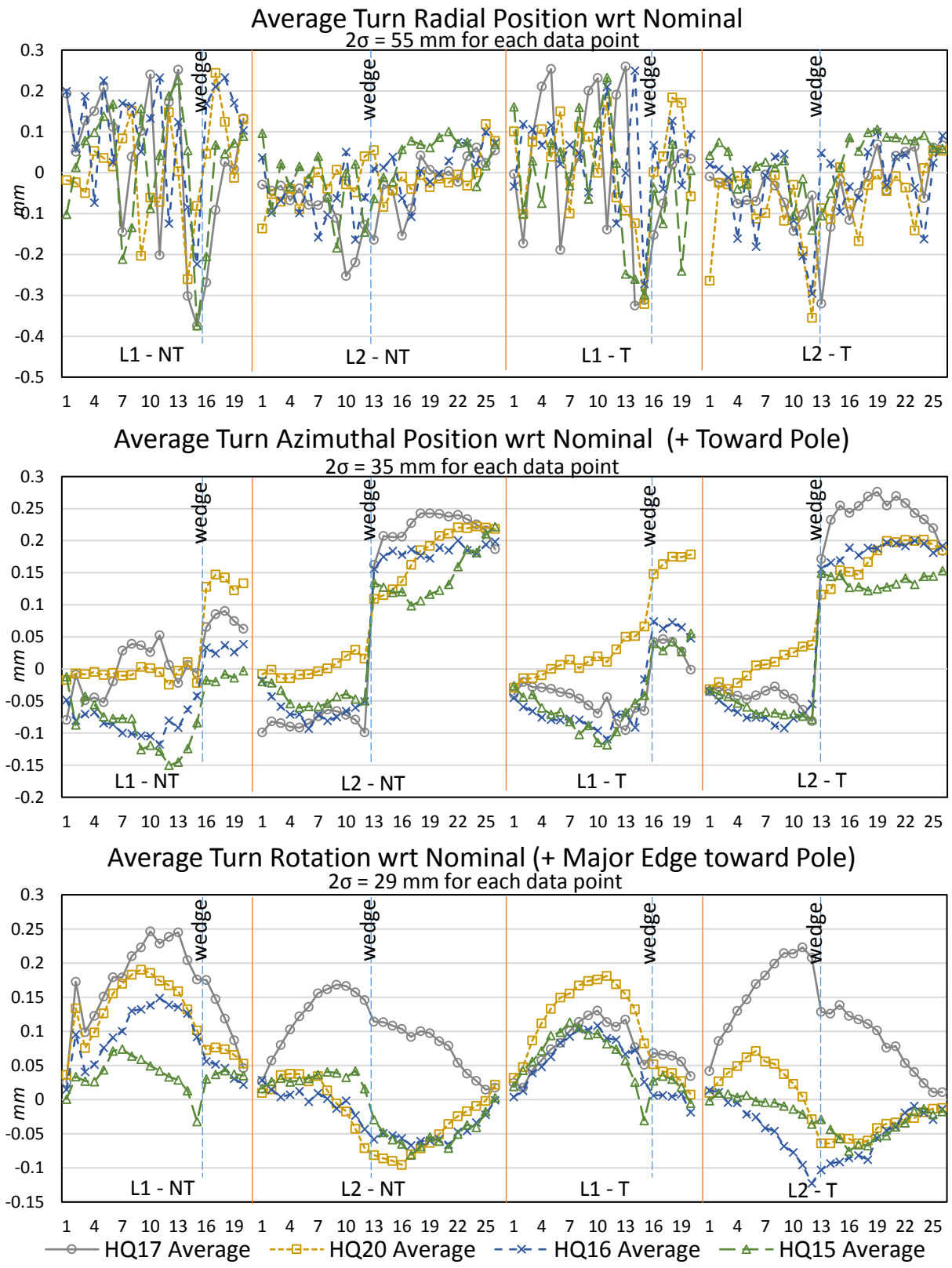

Fig. 13. Average radial, azimuthal, and rotational turn displacements with respect to the nominal position. The 95% confidence level for each measurement is indicated.

Turn rotation for HQ17 is significantly different from the other coils in Fig. 13. HQ17 turns have a strong tendency for the major edge of each turn to rotate toward the pole. This same phenomenon is seen consistently in all of the braided-on insulation QXF practice coils. The rotation of the sock type insulation coils seem to be closer to nominal or even rotating the opposite direction. Braided on insulation allows slightly more thickness or azimuthal growth from increased width constriction which should reduce the azimuthal displacements. However, the braided-on insulation coils have significantly more azimuthal displacement than the sock type coils. This unexpected trend indicates that there is likely some coupling between radial and azimuthal displacements. The idea of this coupling will be discussed more in the next section.

D. Turn and Block Waviness

Longitudinal waviness is defined as the amount that each turn or block shifts as a function of longitudinal position. More specifically, it is the difference in position of a block or turn as measured in two independent cross sections of a coil. In this manner the root mean square waviness for two cross sections that are only one mm apart should be approximately zero. The root mean square waviness for two cross sections that are several meters apart should asymptotically approach some value related to the constraints of the coil cavity. Data was collected from all four coils of HQ02 from cross sections 1, 26, 74, 100, and 200 mm apart. Coil 17 data was split from coils 15, 16, and 20 due to the difference in cable insulation and associated cavity free space as shown in Table II.

The radial waviness in all coils is quite consistent despite the radial free space in HQ17 having roughly 150 µm per layer more radial free space compared to other coils. The bulk of this additional free space is realized by additional turn rotation waviness as seen in Fig. 14 for both the blocks and turns.

The azimuthal free space using sock type insulation is 28 µm per turn or 280 and 364 µm for L1 and L2 while the braid type insulation has zero free space. Sock type coil waviness is 5 times larger than the braided-on insulation of HQ17 as seen in Fig. 14. The azimuthal free space corresponds very well with azimuthal waviness.

More data is being collected to attempt to measure the asymptote of this waviness beyond 200 mm.

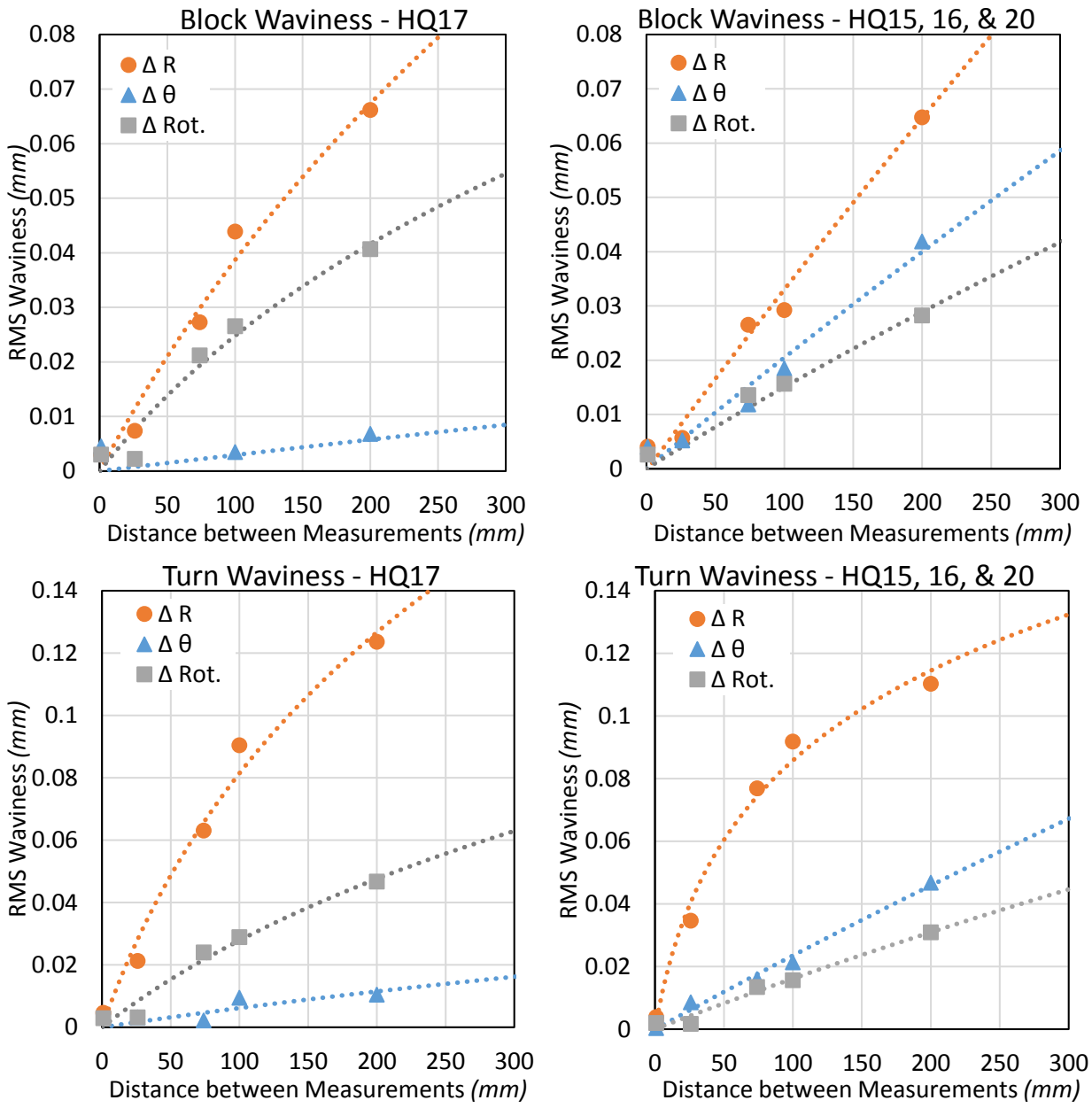

Fig. 14. Block and turn longitudinal waviness. Waviness is defined as the RMS amount a block or turn shifts between measurements that are a certain distance apart.

TABLE II

		Braid (Coil 17)			Sock (Coils 15, 16, & 20)		
		Radial (μm)	Azimuthal (μm)	Rotation (μm)	Radial (μm)	Azimuthal (μm)	Rotation(μm)
Block RMS	Displacement from Nominal	59	125	118	67	111	67
	Displacement from Average	46	36	84	52	48	34
	Waviness 100 mm	41	5	27	30	16	16
	Waviness 200 mm	66	4	40	68	42	29
Turn RMS	Displacement from Nominal	156	138	131	127	114	80
	Displacement from Average	116	46	96	107	49	42
	Waviness 100 mm	90	11	29	92	20	16
	Waviness 200 mm	124	8	46	110	47	31
	Coil Cavity	1.4%	3.9%	-	1.6%	6.0%	-
	Cable Expansion	0.4%	4.4%	-	1.6%	3.8%	-
	Free Space	148 per layer	0	-	0	28 per turn	-

RMS displacement, waviness, and free space of each turn and coil block. Analysis is based on 20 total cross sections. RMS Displacement is the displacement of each block or turn with respect to the nominal position and to the average position of all coils. Waviness is the RMS shift of each turn or block between cross sections 100 and 200 mm apart. The coil cavity is the value that the cable is allowed to expand into. The cable expansion is measured from cable expansion experiments and other cross sections. The free space is the difference between the cavity size and the cable expansion.

The data in TABLE II is a summary of all measurements. The braided on insulation is 104 μm thick and the sock type is 90 μm thick [8]. This differences produces the various coil cavity sizes seen in TABLE II. There is some agreement between radial free space and radial waviness and significant agreement between azimuthal free space and azimuthal waviness. TABLE II provides a baseline for simulating the range of harmonics that should be measured longitudinally along the magnetic length.

VII. Field Variation from Block and Turn Movement

The amount that each harmonic changes longitudinally is determined by how each coil, block, and turn moves laterally or shifts along the magnet. TABLE II in the previous section is useful for estimating the accuracy of how each harmonic should vary along the coil.

A Monte-Carlo code was written in Java to calculate the harmonics based on 36 line currents uniformly distributed within each cable block. The code neglects effects from iron. Random Turn/block/coil shifts are binomially distributed with a standard deviation based on cross sectional data in TABLE II.

At the winding and block level we have radial, azimuthal, and rotational /radial shifts and wedge/turn rotations. From coil cross sections it is evident that there is little azimuthal and rotational error in the position of the midplane and pole turns. Therefore azimuthal and rotational shifts only affect the middle turns of each level near the wedge. A demonstration of each shift is shown in Fig. 11.

The normal and skew RMS harmonics are presented in Fig. 12 as generated by both displacements and waviness. Here the reader is reminded that the RMS harmonics can be calculated by the Root-Mean-Square method and is equivalent to the square root of the square of the average summed with the square of the standard deviation. The total expected RMS harmonics and the actual measured RMS harmonics are presented in Fig. 12 as well. The b3, b10, and a10 measured harmonics are significantly larger than expectation. The b3 harmonic is likely due to relative coil placement rather than turn displacement at the coil level while the b10 and a10 harmonics are possibly due to probe resolution.

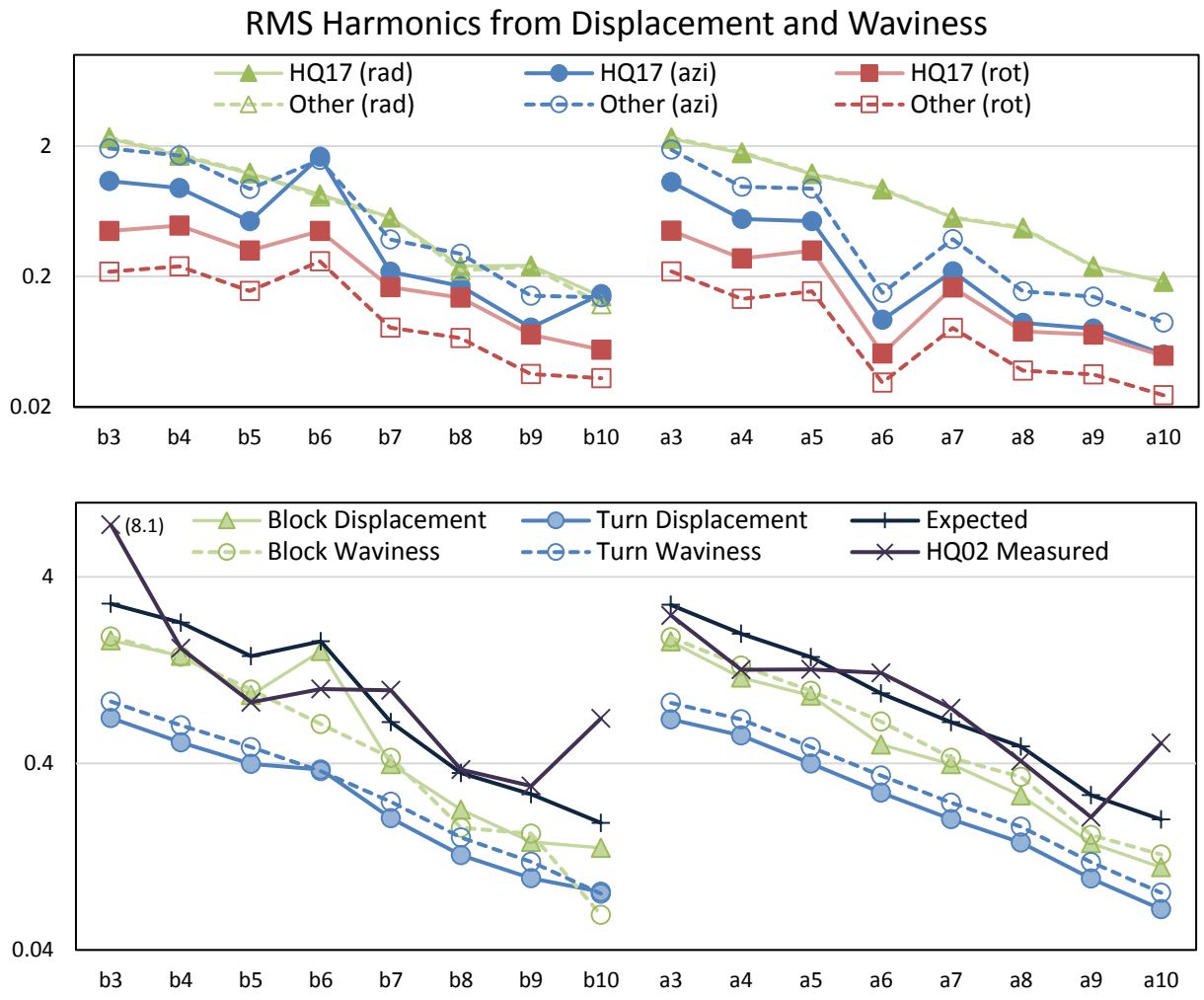

Fig. 12. Normal and Skew RMS harmonics from turn and block displacements and 200 mm RMS waviness as presented in TABLE II. The top graph presents differences between radial, azimuthal, and rotational dimensions while the lower graph presents differences between displacements and waviness. The total expected RMS harmonics and total measured RMS harmonics are presented in the lower graph.

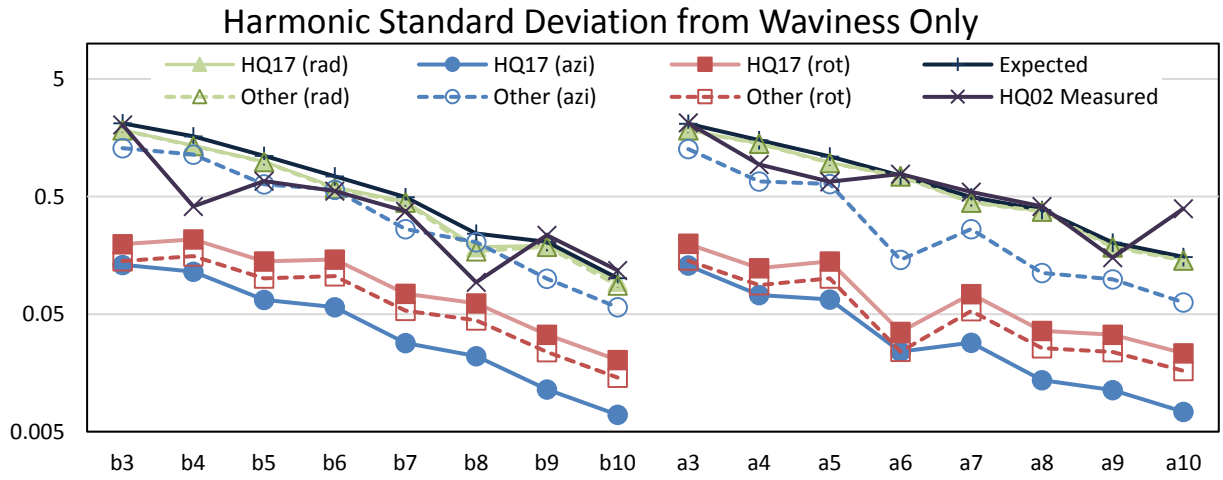

Fig. 13. Normal and Skew RMS harmonics from 200 mm RMS waviness as presented in TABLE II. The total expected and measured harmonic standard deviations are also plotted. The total expected harmonic standard deviation is purely from conductor waviness.

The harmonic standard deviations are presented in Fig. 13 and are due to waviness only. Average turn displacement contributes to the harmonic magnitude but not the standard deviation. The measured harmonic standard deviation is based on 400 mm of uniform field while the calculated standard deviation is from 200 mm waviness data from TABLE II. The measured harmonic standard deviation is on average 0.17 units smaller than what was calculated and corresponds to waviness values 21% smaller than what is given in TABLE II.

Another approach to the waviness analysis is to compare changes in field and waviness at same intervals. In Fig. 14 the changes in harmonics at 200 mm intervals are plotted along with the expected changes in harmonics from 200 mm waviness data given in TABLE II. Comparing the data in this manner decreases the agreement between measurement and expectation but perhaps is a better representation of the effect of waviness. The measured RMS harmonic change is on average 0.25 units larger than what was calculated and corresponds to waviness values 28% larger than what is given in TABLE II.

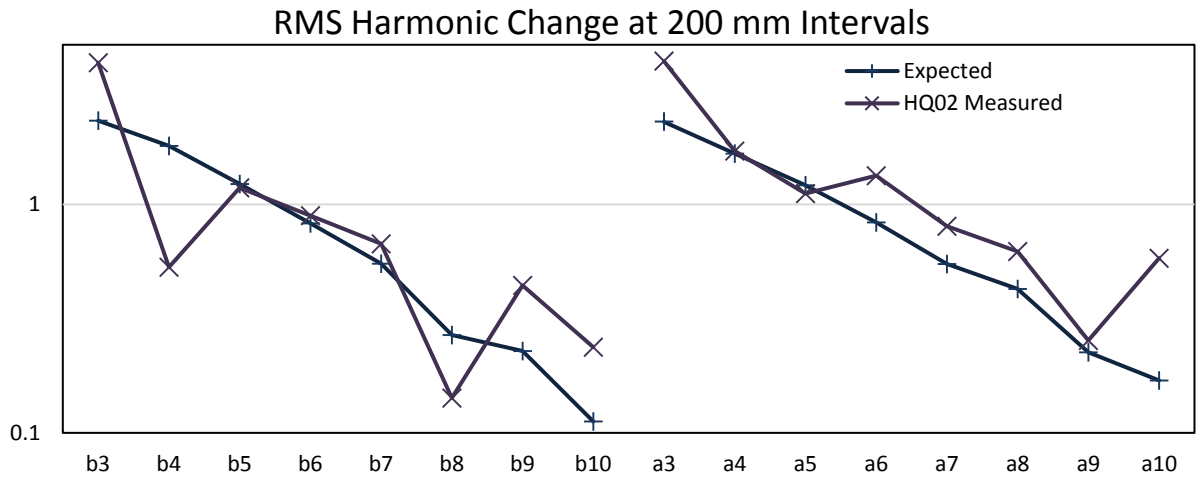

Fig. 14. Normal and skew RMS harmonic changes at 200 mm intervals. The expected change is calculated from 200 mm waviness data.

The effects from waviness are essentially uncertainties associated to correlating magnetic field measurements with a rotating coil to the magnetic field calculations based from magnet cross section. These uncertainties are included in the next section.

VIII. Magnetic field from Collared Coil Cross Sections

Three full cross section have been assembled using coils HQ17, HQ16, HQ15, and HQ20 from the first quadrant counterclockwise. The four coils have been assembled with four collars, meeting the requirement of 100 in-lbs. torque for bolts. The cross sections analyzed were at z = -5, -79, -105 as referenced in Fig. 6. For z = -79, the cross section is seen from trailing or return end of the magnet, so points have been flipped around the 45° line to be comparable with other cross sections as shown in Fig. 15.

All previous consideration apply to the process of collecting data points, except for the reference frame setting: the keyways of the four coils were used without the OD. For each keyway the center was computed as mentioned before and the center of the reference frame was set at the intersection of the line passing through opposite keyway centers.

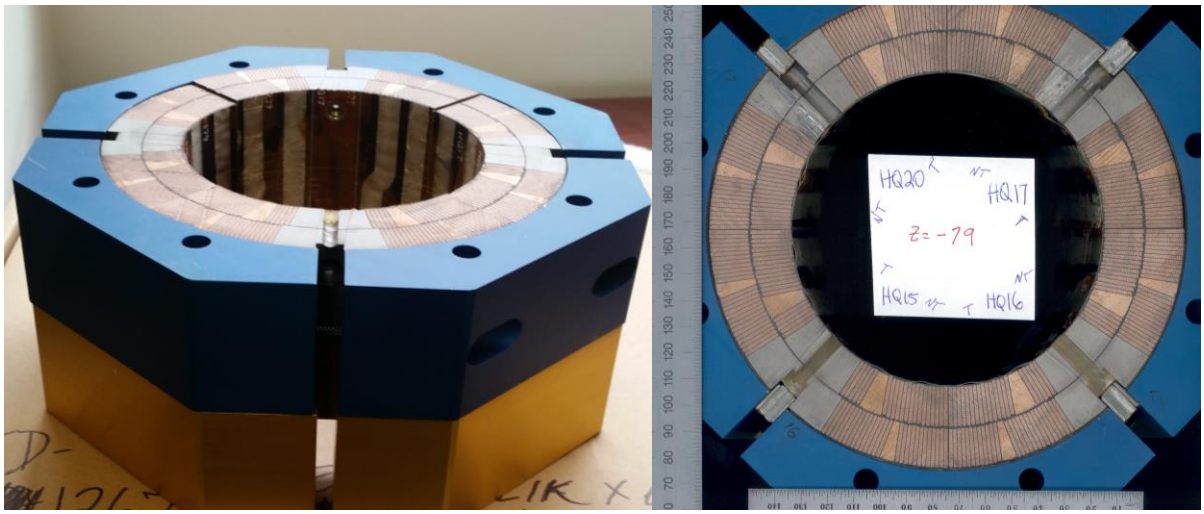

Fig. 15. Picture and scan of HQ02 cross section

A. Current Location inside each turn

In order to use the measured turn locations to compute magnetic field, the position of individual line currents was computed. The cable is simulated as having 36 strands, divided in two rows with 18 strand each. The actual process of finding the current locations is the following:

$$\mathbf{P}_{1j} = \frac{1}{4}(2j-1)x_1 + \left(1 - \frac{1}{4}(2j-1)\right)x_2 \qquad j = 1,2 \tag{15}$$

$$\mathbf{P}_{2j} = \frac{1}{4}(2j-1)x_3 + \left(1 - \frac{1}{4}(2j-1)\right)x_4 \tag{16}$$

$$x_{ij} = \mathbf{P}_{1j} + \frac{(\mathbf{P}_{2j} - \mathbf{P}_{1j})}{36}(2i-1) \qquad i = 1, \ldots, 18 \tag{17}$$

The magnetic field is calculated using COMSOL with the iron properties equal to the magnetization chart used in OPERA. Various comparisons of COMSOL with OPERA and ROXIE were performed with indistinguishable results. [9]

B. Magnetic Field Measurement and Calculation

The measured harmonics are presented in the Fig. 16 and the calculated harmonics are presented in Fig. 17. The measured harmonics are from a 100 mm long rotating coil and calculated harmonics are from full magnet cross sections. The calculated harmonics are from COMSOL and measured turn placement as input. Measured harmonics vary little between z=-5 and z=-105 due to the smoothing, integral nature of the 100 mm rotating coil. The calculated field from single cross sections has larger variation. In Fig. 16, measured harmonics from the rotating coil vary gradually along the length of the coil as indicated by how close the cold data at -5 mm and -105 mm are to each other.

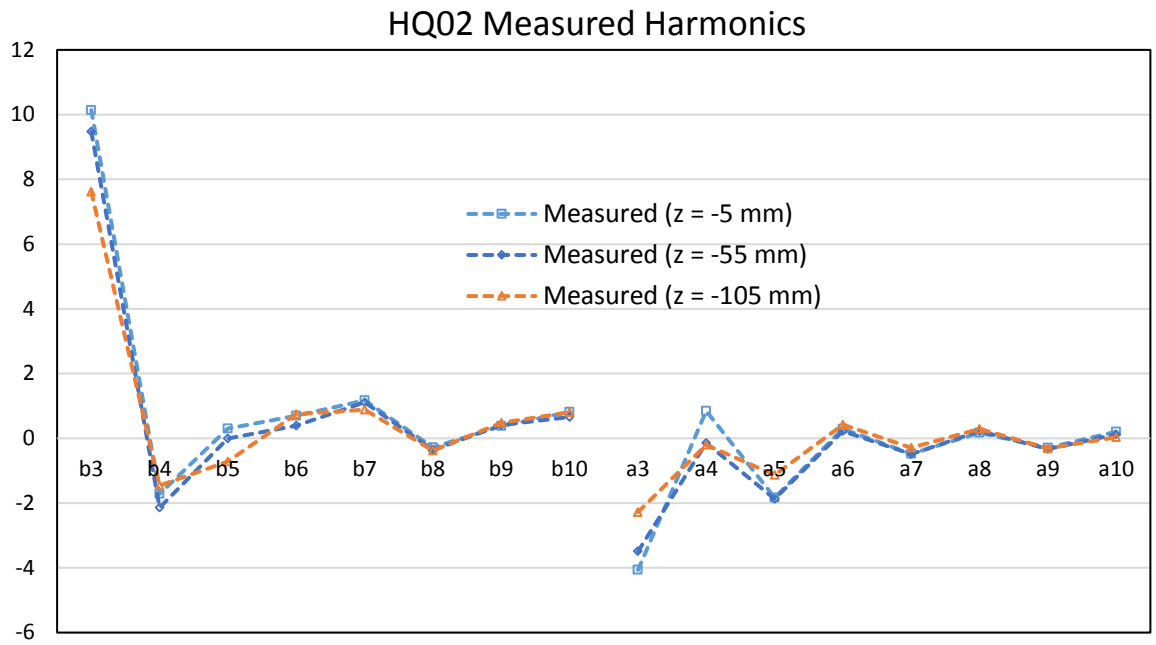

Fig. 16. Measured Normal and Skew multipoles from the rotating coil at 14.6 kA and 1.9 K.

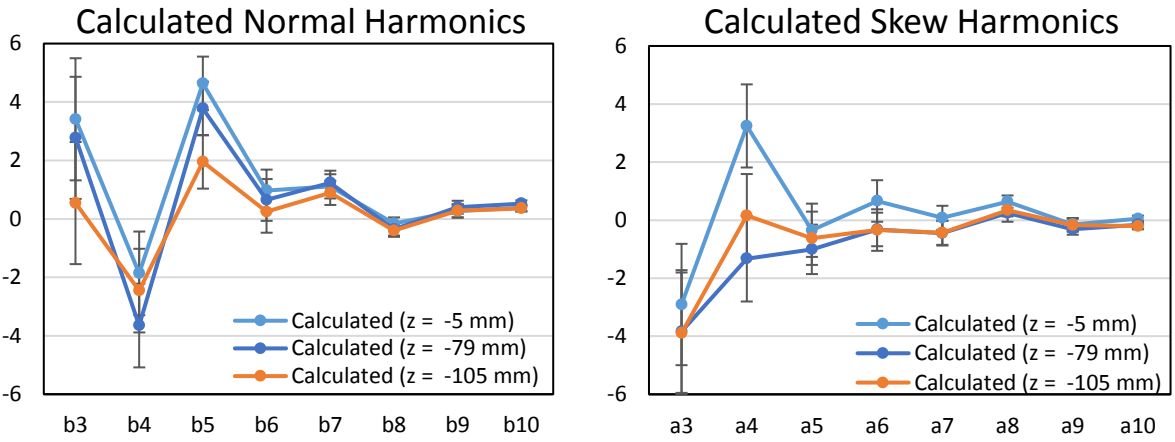

Fig. 17. Calculated normal and skew multipoles from full cross sections of HQ02 at 14.6 kA. The error bars are from 100 mm waviness data.

Although every very effort was taken to replicate the as assembled coils there remains significant variability in relative coil positioning and is demonstrated by increased variability in calculated harmonics. Large variability in a4 strongly indicates that coil loading in the collars is not uniform. Fig. 18 shows the contribution that each strand of current has on the a4 harmonic. Any oblong type deformation directly effects a4 and is difficult to control without the full magnet structure preload.

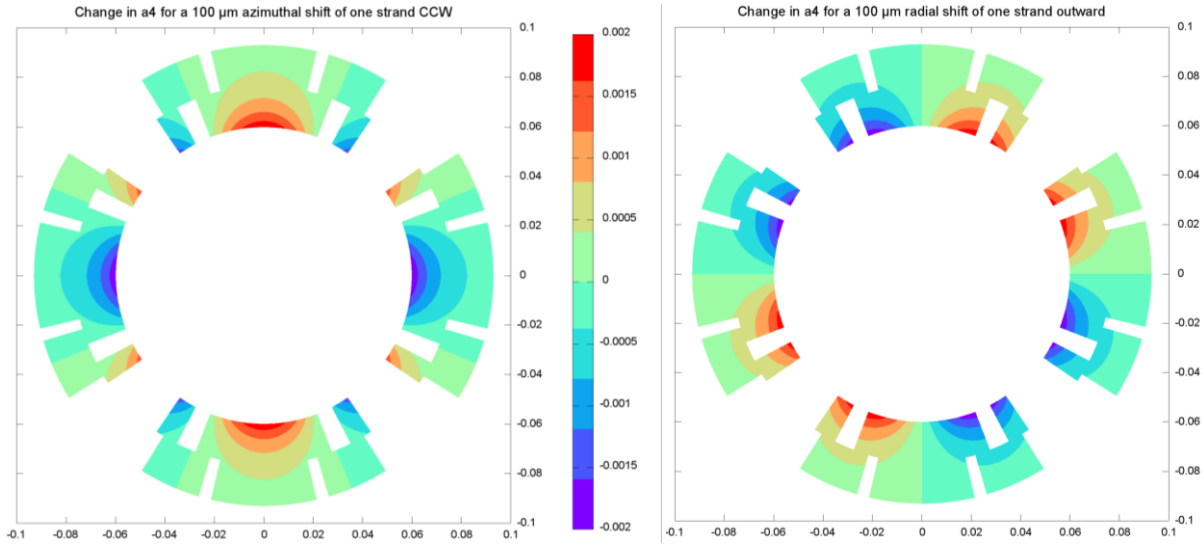

Fig. 18. Contribution of each strand to the a4 harmonic in HQ02.

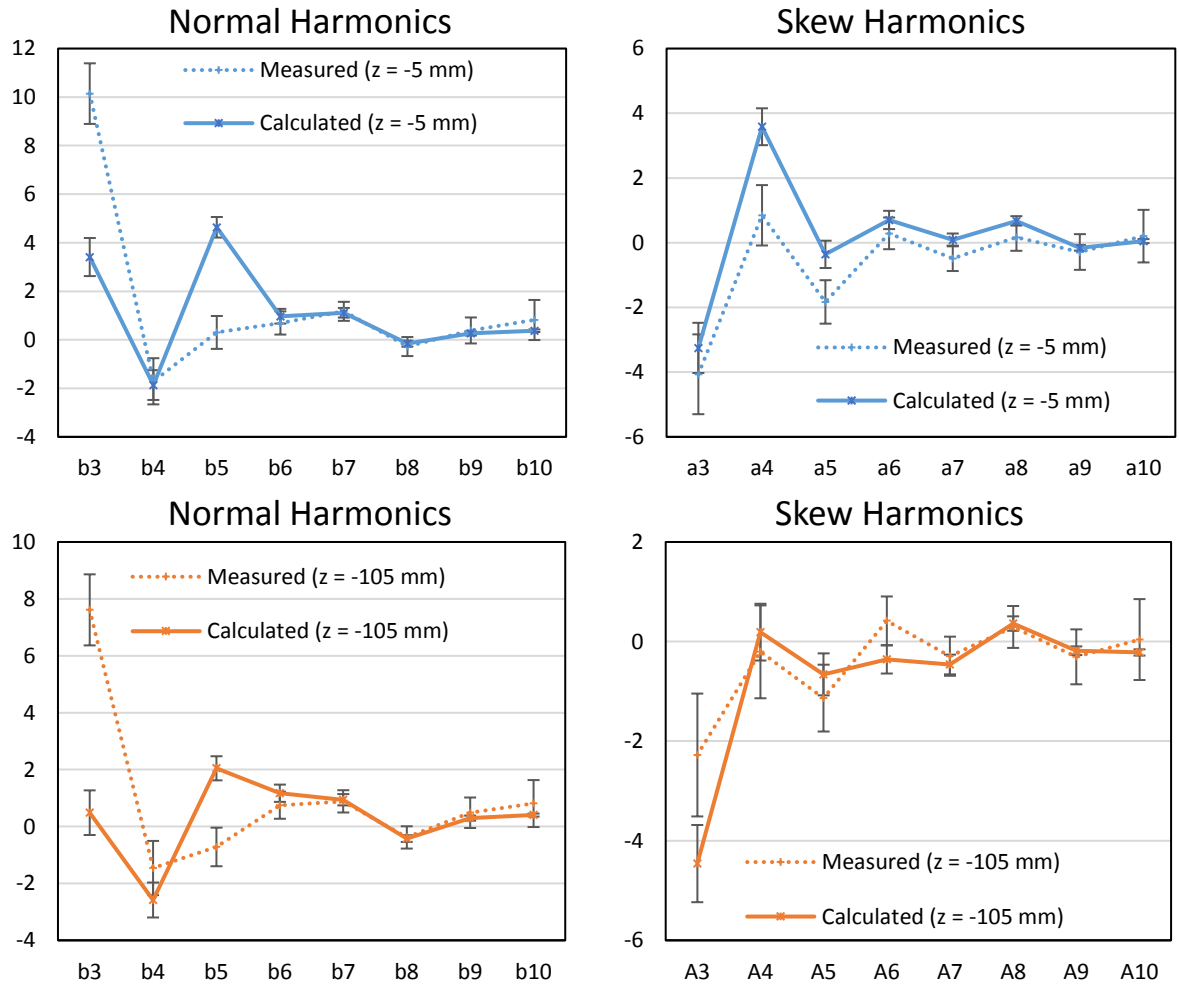

Fig. 19. Calculated and measured normal and skew harmonics at z = -5 mm and 105 mm. Measured harmonics are from a 100 mm rotating coil at 14.6 kA and 1.9 K. The calculated harmonics are from turn measurement and COMSOL.

In Fig. 19 we have a comparison of the calculated and measured harmonics taken at -5 mm and -105 mm. The correlation between measured and calculated harmonics is relatively weak. Using the Student's T-Test formula, $\frac{|A_{n_{measured}} - A_{n_{calculated}}|}{\sqrt{\sigma^2_{A_{nMeasured}} + \sigma^2_{A_{nCalculated}}}}$, the average value is 1.13. The T-Test indicates a confidence level of 28% for correlation between the warm 10A data measurement and the cross section calculation. In other words the measured and calculated harmonics differ at the 72% confidence level.

For a quadrupole the field has 180 degree rotational symmetry. This 'quad ambiguity' allows the odd harmonics to change sign while the even harmonics are unaffected due to symmetry. If the odd harmonics are flipped the correlation jumps from the 28% confidence level to the 48% confidence level.

IX. Conclusions

Turn locations were measured at several cross sections of HQ02 by a coordinate measuring optical comparator. A rotation and translation minimization process enabled repeatability and accuracy of measurement to within 15 µm.

Turns and coil blocks tend to be radially displaced with respect to nominal by RMS values of 130 µm and 60 µm. Turns and blocks both have an RMS azimuthal displacement of 130 µm. Displacements in coil HQ17 are ~10% larger than the other coils largely due to braided on insulation constricting lateral growth.

RMS Shifts in turn placement are in excess of 100 µm at distances of only 100 mm along the length of the coil. Peak shifts are as much as 500 µm. Large displacements and movements likely inhibit accurate correlation between measured harmonics and calculated harmonics from turn measurement.

The positional analysis of individual turns, blocks, and coils correlate well with measured harmonics. The magnitude and the RMS variation of each harmonic agree well with the amount of RMS displacement and waviness seen from individual coil cross sections.

The correlation between a full magnet cross section and the actual measured harmonics is weak. The weak correlation is partly due to the measured harmonics being an average based on the length of the harmonic probe while the cross section is a point like assessment of turn position. Each full magnet cross section was assembled with only the aluminum collars and do not constrain the coils like the full magnet structure further contributing to a weak correlation between simulated field from a full cross section and a the measured field.

X. References

[1] E. Todesco, et al., "Design studies for the low-beta quadrupoles for the LHC luminosity upgrade," IEEE Trans. App. Supercond., vol. 23, no. 3, p. 4003305, June 2013.

[2] Original LARP Proposal, 2003, http://www.uslarp.org/LARP_Proposal.pdf

[3] F. Borgnolutti, et al., "Fabrication of a Second-Generation of Nb3Sn Coils for the LARP HQ02 Quadrupole Magnet," IEEE Trans. App. Supercond., vol. 24, no. 3, p. 4003005, June 2014.

[4] G. Chlachidze, et al., “Performance of HQ02, an Optimized Version of the 120 mm Nb3Sn LARP Quadrupole,” IEEE Trans. App. Supercond., vol. 24, no. 3, pp.1-5, June 2014.

[5] S. Caspi, et al., “Design of a 120 mm Bore 15 T Quadrupole for the LHC Upgrade Phase II,” IEEE Trans. Appl. Supercond., vol. 20, no. 3, pp. 144-147, June 2010.

[6] J. DiMarco, et al., “Field Quality Measurements of LARP Nb3Sn Magnet HQ02,” IEEE Trans. App. Supercond., vol. 24, no. 3, p4003905, June 2014.

[7] H. Bajas, et al., “Test Results of the LARP HQ02b Magnet at 1.9 K,” IEEE Trans. App. Supercond., vol. 24, no. 3, pp.1-5, June 2014.

[8] F. Borgnolutti, et al., “Fabrication of a Third Generation of Nb3Sn Coils for the LARP HQ03 Quadrupole Magnet,” IEEE Trans. App. Supercond., vol. 24, no. 3, p. 4002505, June 2014.

[9] I. Rodriguez and J.L. Munoz, “Benchmark of COMSOL vs. ROXIE Codes for the Calculation of a Particle Accelerator Quadrupole,” Excerpt from the Proceedings of the 2011 COMSOL Converence3 in Stuttgart, https://www.comsol.com/paper/download/83731/rodriguez_paper.pdf Downloaded August 2016.